Stability Enhancement and Feedforward Power-Constrained Control for SWPDT Systems Under Source–Load Power Fluctuations

Yongling Lu[1], Zhitong Xue[1], Jiahao Guo[1], Zhijun Wu[2], Xin Fang[1], Rui Zhu[1], Linlin Tan[2]*
[1]Jiangsu Electric Power Company Electric Power Research Institute, Nanjing, China
[2]School of Electrical Engineering, Southeast University, Nanjing, China

Corresponding author: Linlin Tan (e-mail: tanlinlin@seu.edu.cn).

ABSTRACT This paper investigates the stability problem of a series-series compensated wireless power transfer distribution (SWPDT) system under source–load power fluctuations. First, a source-side power harvesting model is established, revealing the nonlinear constrained characteristic of available power with respect to transmission line current. Furthermore, the input-side equivalent negative impedance characteristic under constant-voltage control is analyzed, which amplifies source–load disturbances and deteriorates dynamic power stability. Based on this, the DC bus energy balance model is developed to reveal the positive feedback mechanism induced by power mismatch, and the degradation mechanism of ZVS conditions and switching failure is further investigated. To address the instability issue, a feedforward power-constrained control strategy based on source-side available power information is proposed. By incorporating real-time source power capability into the control loop, the input current reference is actively constrained, ensuring that the system input power is always bounded by the source-side harvesting capacity, thereby mitigating the power over-regulation problem inherent in conventional constant-voltage control. Experimental results demonstrate that the proposed method effectively suppresses DC bus voltage collapse, improves dynamic response performance, and significantly enhances system stability under source–load power fluctuation conditions.

INDEX TERMS Transmission line energy harvesting; wireless power transfer; source–load interaction; feedforward power-constrained control; DC bus dynamics; dynamic stability

I. INTRODUCTION

The harvesting of energy from transmission lines has proven to be an effective means of powering distributed sensing units within the context of modern electrical networks. As one of the examples of such technologies, the series-series compensated wireless power transfer distribution (SWPDT) system has been designed to monitor line energy retrieval via the electromagnetic induction of line currents [1]–[3]. Such systems enable continuous power supply to sensing and communication devices along transmission lines, which increases the reliability and autonomy of distributed monitoring networks [4]–[7].

In an effort to improve SWPDT system capabilities, the simultaneous transfer of power and data via a single channel has been widely studied [8]–[10]. Most of the existing methods of cooperative transmission of power and data are based on the combination of carrier injection and energy modulation [11]–[14]. In the case of carrier injection methods, information is conveyed by the superimposition of a high-frequency communication signal onto the power transfer process, which enables high communication rates. However, it is often necessary to use additional filtering devices and modulation/demodulation circuits, which increases the cost of the system and its complexity [15]–[17]. In comparison, systems based on energy modulation are advantageous because they offer low complexity. However, the embedded information to be conveyed with the power to be transferred can be adversely affected if there are fluctuations in the power transfer conditions.

In practical transmission line operating environments, the harvested power of SWPDT systems is highly dependent on grid operating conditions. The transmission line current varies continuously due to load fluctuations and switching operations of electrical equipment, leading to corresponding variations in the available harvested energy [18]–[21]. Therefore, the power supply capability of the energy harvesting unit cannot be regarded as constant, but exhibits time-varying characteristics under different operating conditions. When the line current decreases, the available harvesting power is reduced accordingly, introducing uncertainty in the energy supply capability. Meanwhile, the receiver-side DC–DC converter generally adopts constant-voltage control to maintain stable output [22]–[24]. Under varying input voltage conditions, this control strategy adjusts the input current demand, leading to strong dynamic interactions on the input side of the system.

Under the combined effects of source-side power fluctuations and load-side control dynamics, SWPDT systems are prone to power supply–demand mismatch under fast disturbance conditions [25]–[27]. Conventional voltage-based feedback control methods rely on post-event voltage information, resulting in inherent response delays and limited effectiveness in highly dynamic scenarios [28]–[30].

To address these issues, this paper proposes a feedforward power-constrained control strategy based on source-side power information. A feedforward power-constrained control strategy is proposed by incorporating source-side power information, which enables adaptive input current regulation and improves stability under power fluctuations.

The main contributions of this work are summarized as follows:

(1) A dynamic power constraint model of transmission line energy harvesting systems is developed to characterize the nonlinear dependence of available power on line current;
(2) The input-side behavior under constant-voltage control is analyzed, revealing the impact of source–load dynamic interaction on system power balancing;
(3) A feedforward power-constrained current reference control method is proposed, which explicitly incorporates power constraints into the control architecture and improves system robustness against power fluctuations.

II. SYSTEM MODEL AND SOURCE–LOAD POWER CHARACTERISTICS

A. SYSTEM STRUCTURE AND ENERGY TRANSFER MECHANISM

The series–series wireless power transfer distribution system with power regulation and information coupling (SWPDT) is designed for transmission line monitoring and power supply applications. The overall system architecture is illustrated in Figure 1.

The system consists of a CT-based energy harvesting unit, a front-end rectification and power conditioning stage, a half-bridge inverter, an SS-compensated wireless power transfer link, a receiver-side rectifier, a DC/DC conversion stage, and a monitoring load.

The transmission line current is first converted into electrical energy through the CT-based harvesting unit. After rectification, a DC bus voltage U_{in} is established to supply the inverter, which generates high-frequency AC excitation for wireless energy transfer. The transmitted power is delivered through a magnetic coupling link and finally regulated at the receiver side to provide a stable DC output for the load.

A key characteristic of the system is that the source-side input power is determined by the operating condition of the transmission line, exhibiting strong time-varying and power-limited behavior.

B. SOURCE-SIDE POWER CONSTRAINT CHARACTERISTICS

To characterize the power limitation behavior of the source-side energy harvesting unit, the relationship between transmission line current and harvested power is first analyzed.

Let the transmission line current be expressed as:

$$i_1(t) = I_{1m}\sin(\omega t) \tag{1}$$

The harvested voltage generated by the CT-based energy harvesting unit can be described as:

$$u_c = f(I_1) \tag{2}$$

Based on this relationship, the source-side available power is defined as:

$$P_{avail} = f(I_1) \tag{3}$$

To describe more the characteristics of the power limitation, it is necessary to conduct experiments to determine the maximum obtainable harvesting power under various line current situations.

The maximum available power can be expressed as:

$$P_{\max} = \alpha I_1^{\beta} \tag{4}$$

where α and β represent the parameters set by the harvesting structure with the corresponding operating conditions.

The system input power is defined as:

$$P_{in} = U_{in}I_{in} \tag{5}$$

When facing power restrictions from the source side, the system must fulfill this constraint:

$$U_{in}I_{in} \le P_{avail} \tag{6}$$

To visually illustrate the relationship between transmission line current and the harvested energy capability, the corresponding experimental results are shown in Figure 2.

The findings show that the maximum limit of the harvesting power increases nonlinearly as a function of the transmission line current, demonstrating how the harvesting potential is heavily influenced by an operating scenario. The power source-side limitation establishes the primary boundary of system function, which supports source–load coupling and stability assessment.

C. LOAD-SIDE DYNAMICS AND DC BUS ENERGY INTERACTION

The DC/DC converter on the receiver side uses constant-voltage control as its operational strategy. The output power can be formulated as:

$$P_{out} = \frac{U_{out}^2}{R} \tag{7}$$

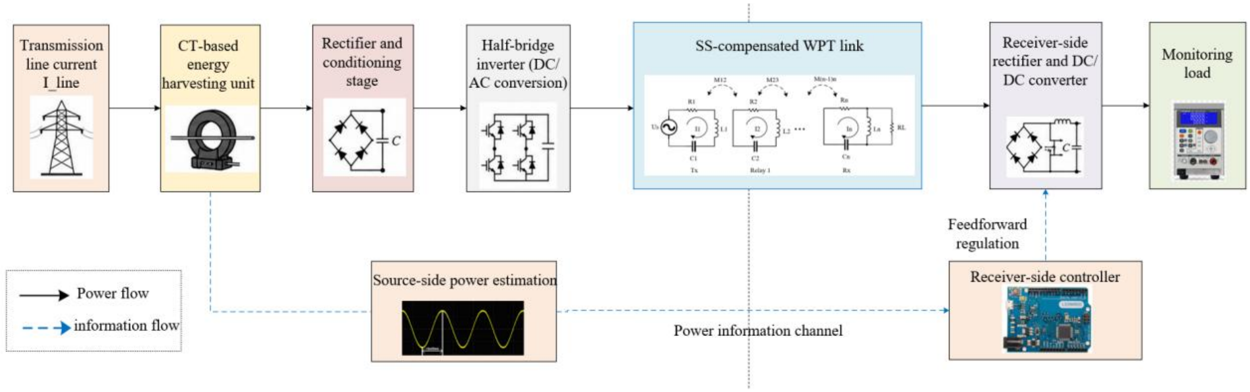

FIGURE 1. System architecture of SWPDT.

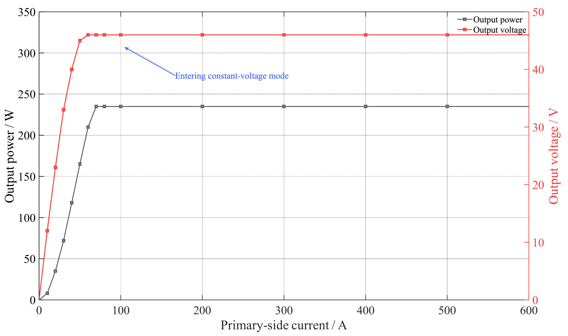

FIGURE 2. Relationship between primary current and harvested power/voltage.

Neglecting converter losses, the input and output powers satisfy:

$$P_{in} \approx P_{out} \tag{8}$$

Thus, the input current can be derived as:

$$I_{in} = \frac{P_{out}}{U_{in}} \tag{9}$$

This relationship indicates that under constant-voltage control, a reduction in input voltage leads to an increase in input current demand, revealing an inherent coupling effect between the load-side regulation behavior and the input electrical dynamics.

To further describe the system dynamic behavior, the DC bus stored energy is expressed as:

$$E_{dc} = \frac{1}{2} C U_{dc}^2 \tag{10}$$

Taking the time derivative yields the DC bus power balance equation:

$$C U_{dc} \frac{dU_{dc}}{dt} = P_{in} - P_{out} \tag{11}$$

This equation reveals that the DC bus voltage dynamics are directly governed by the power imbalance between the source-side input power and the load-side demand.

When $P_{in} < P_{out}$, the DC bus capacitor discharges to sustain the load, resulting in a continuous decrease of U_{dc}. This process indicates that the system enters an energy-deficient state, in which the load-side regulation behavior further amplifies the power imbalance through increased input current demand. This coupling behavior leads to dynamic instability under power fluctuation conditions, which is analyzed in detail in Section 3.

III. STABILITY MECHANISM AND INSTABILITY ANALYSIS UNDER SOURCE–LOAD COUPLING

A. SOURCE-SIDE POWER CONSTRAINT CHARACTERISTICS

In the SWPDT system, the energy harvesting unit is directly driven by the transmission line current, and its output capability is inherently constrained by the operating state of the line. Therefore, the source-side power exhibits a nonlinear and time-varying limitation characteristic.

The transmission line current is expressed as:

$$i_1(t) = I_{1m} \sin(\omega t) \tag{12}$$

The harvested voltage of the CT-based energy harvesting unit is described as:

$$u_c = f(I_1) \tag{13}$$

The source-side available power is defined as:

$$P_{avail} = f(I_1) \tag{14}$$

Based on experimental fitting, the maximum harvesting capability is given by:

$$P_{\max} = \alpha I_1^{\beta} \tag{15}$$

The system input power is defined as:

$$P_{in} = U_{in} I_{in} \tag{16}$$

Thus, the source-side operating constraint can be formulated as:

$$P_{in} \leq P_{avail} \tag{17}$$

To illustrate the nonlinear relationship between line current and harvesting capability, the experimental results are shown in Figure 3.

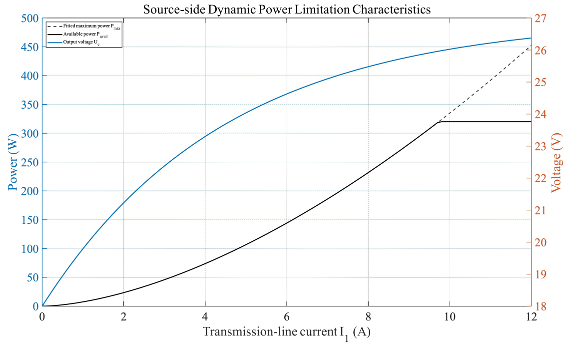

FIGURE 3. Source-side power constraint characteristic under varying line current.

The results indicate that the harvesting capability is fundamentally bounded by the operating condition of the transmission line, forming the first-order constraint of system stability.

B. NEGATIVE IMPEDANCE CHARACTERISTIC UNDER CONSTANT-VOLTAGE CONTROL

The receiver-side DC/DC converter operates under a constant-voltage control strategy. The output power is expressed as:

$$P_{out} = \frac{U_{out}^2}{R} \tag{18}$$

Neglecting converter losses, the power balance is:

$$P_{in} \approx P_{out} \tag{19}$$

Thus, the input current is given by:

$$I_{in} = \frac{P_{out}}{U_{in}} \tag{20}$$

The incremental relationship between input current and input voltage satisfies:

$$\frac{\partial I_{in}}{\partial U_{in}} < 0 \tag{21}$$

Therefore, the equivalent input impedance is:

$$Z_{in} < 0 \tag{22}$$

To validate this characteristic, the experimental results are shown in Figure 4.

This result indicates that the load-side regulation mechanism introduces an inherent negative impedance behavior, which reduces system damping and weakens the ability to suppress disturbances.

C. POWER MISMATCH AND DC BUS DYNAMIC EVOLUTION

The energy stored in the DC bus is expressed as:

$$E_{dc} = \frac{1}{2} C_{dc} U_{dc}^2 \tag{23}$$

The dynamic power balance equation is:

$$C_{dc} U_{dc} \frac{dU_{dc}}{dt} = P_{in} - P_{out} \tag{24}$$

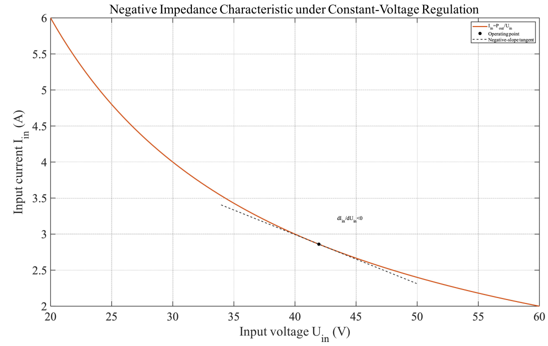

FIGURE 4. Negative impedance characteristic under constant-voltage control.

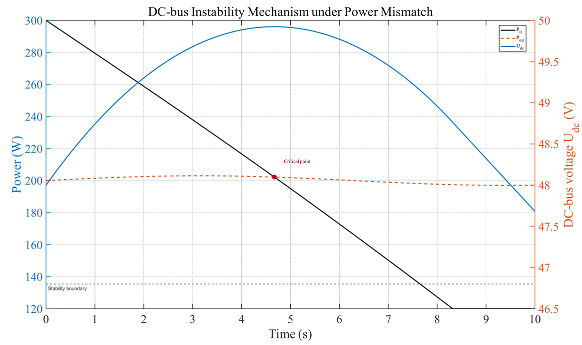

FIGURE 5. DC bus voltage collapse mechanism under power imbalance.

The system enters a mismatch state when:

$$P_{in} < P_{out} \tag{25}$$

In this condition, the DC bus capacitor discharges to maintain power delivery, resulting in a continuous reduction of U_{dc}.

The system becomes unstable when the operating point enters the region Ω_{inst}, where the source-side power is insufficient to support the load demand:

$$\Omega_{inst} = \{(P_{in}, P_{out}) \mid P_{in} < P_{out}\} \tag{26}$$

To validate this instability mechanism, the experimental results are shown in Figure 5.

The results demonstrate that system stability is governed by the real-time balance between source-side capability and load-side demand, rather than static operating conditions.

D. ZVS DEGRADATION AND SWITCHING FAILURE MECHANISM

For the inverter to achieve zero-voltage switching (ZVS), the following condition must be satisfied:

$$I_{OFF} > I_{crit} \tag{3-16}$$

where I_{crit} is determined by device parasitic capacitance.

The resonant tank current is a function of available source power:

$$I_{OFF} = h(P_{avail}) \tag{3-17}$$

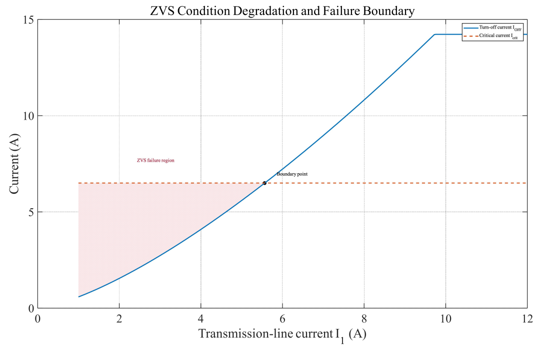

FIGURE 6. ZVS degradation and switching failure boundary.

where $h(\cdot)$ is a monotonically increasing function. ZVS operation is maintained only when:

$$P_{avail} \geq P_{crit} \tag{3-18}$$

When the system enters a power-limited state:

$$P_{avail} < P_{crit} \tag{3-19}$$

the following condition is violated:

$$I_{OFF} \leq I_{crit} \tag{3-20}$$

leading to loss of ZVS operation and transition to hard-switching mode.

To illustrate this boundary, the experimental results are shown in Figure 6.

This phenomenon indicates that switching failure is fundamentally induced by insufficient resonant energy, which originates from source-side power limitation.

IV. FEEDFORWARD POWER-CONSTRAINED CONTROL AND EXPERIMENTAL VALIDATION

A. FEEDFORWARD POWER-CONSTRAINED CONTROL STRUCTURE

Based on the analysis in Section III, the SWPDT system is prone to DC bus voltage collapse under source–load power fluctuations, particularly when the input power continuously approaches the upper bound of the source-side capability. This is mainly due to the fact that the load-side constant-voltage control dominates the input power demand, leading to potential power imbalance under source-limited conditions.

To address this issue, a feedforward power-constrained control strategy is proposed in this paper. By introducing real-time source-side available power information into the receiver-side control loop, the input power demand is actively constrained according to the source capability, thereby preventing the instability mechanism identified in Section III.

The overall control architecture is illustrated in Figure 7.

In this structure, the source-side available power is transmitted through the information channel and used to constrain the current reference according to the source capability.

B. MECHANISM OF FEEDFORWARD POWER CONSTRAINT REGULATION

Under conventional constant-voltage control, the input current is regulated only according to the output voltage error, and the source-side power capability is not considered in the control process. Therefore, the input power may exceed the available harvesting capability under source-side power fluctuations.

To overcome this limitation, a feedforward power constraint mechanism is introduced by incorporating the source-side available power into the current reference generation. The allowable input power is determined by the source capability and load demand, and the corresponding current reference is obtained according to the constrained power level and input voltage.

Through this mechanism, the input power is no longer solely dominated by the load-side requirement, but is jointly regulated by the source capability and load demand. Therefore, the proposed strategy transforms the conventional demand-driven regulation into a source-aware power-constrained control framework.

The results demonstrate that the source-side power information is fed forward to the controller, allowing the input power constraint to be directly incorporated into the control process.

C. STABILITY IMPROVEMENT MECHANISM

Without the proposed feedforward power constraint, the input power is mainly regulated according to the load demand. Under source-side power fluctuations, this demand-driven regulation may cause excessive input current and aggravate the power imbalance, resulting in DC bus voltage instability.

With the proposed strategy, the source-side available power is introduced as a constraint for current reference generation. The input current is therefore regulated within the allowable range determined by the harvesting capability, preventing excessive power demand under source-limited conditions.

Consequently, the power mismatch between the source and load is effectively reduced, and the DC bus energy variation is maintained within a stable operating range. The proposed control strategy suppresses the positive feedback process responsible for voltage collapse and improves the stability of the SWPDT system under power fluctuations.

D. EXPERIMENTAL PLATFORM AND SYSTEM CONFIGURATION

An experimental platform has been constructed to prototype the proposed control strategy. The prototype includes a transmission-line energy harvesting unit, a half-bridge inverter, an SS-compensated wireless power transfer link, an S-BAR modulation and rectification module, and a programmable load DC/DC converter.

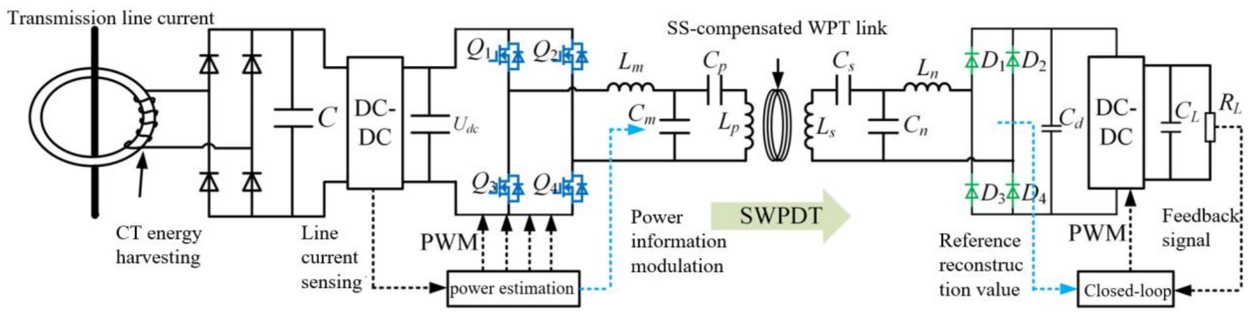

FIGURE 7. Cooperative feedforward power-constrained control structure of the SWPDT system.

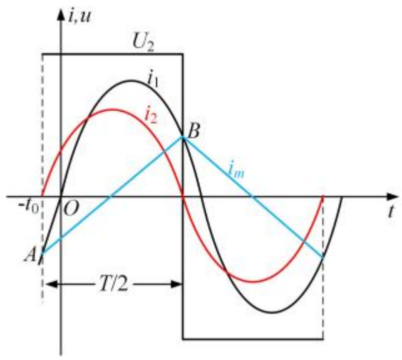

FIGURE 8. Mapping relationship between source-side power information and control input.

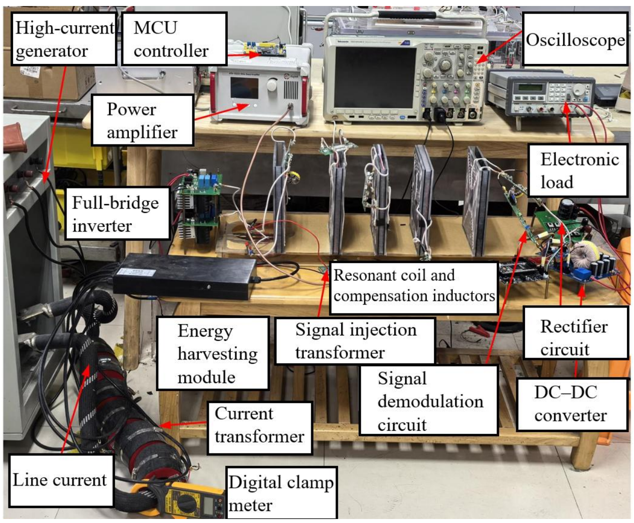

FIGURE 9. Experimental platform of the SWPDT system.

The experimental platform is built on the system configuration and control architecture outlined in Section 2, and the corresponding prototype setup is depicted in Figure 9.

Control parameters have been selected per the theoretical analysis, further refined for experimental application, and ensure that the analytical results match the experimental findings.

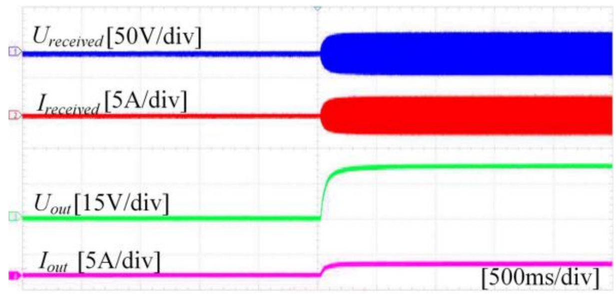

FIGURE 10. System start-up response.

E. EXPERIMENTAL RESULTS AND ANALYSIS

1) START-UP PERFORMANCE

In the startup test, the output voltage and current references were configured to the system at 24 V and 2 A, respectively. The resultant startup waveforms are displayed in Figure 10.

The resultant waveforms show that the output current has a steady-state increase that is achieved in ~400 ms. The absence of noticeable oscillations or overshoot during the transient response demonstrates the proposed control strategy's ability to achieve a stable start-up response.

2) LOAD DISTURBANCE RESPONSE

A load disturbance test was performed by imposing step changes to the load resistance using an electronic load between 12 Ω and 16 Ω. The resultant waveforms are shown in Figure 11.

The waveforms captured show that the output voltage, during the load variation, only experiences a small momentary change and goes back to the steady state value after 50ms. This proves the fast recovery during disturbance, which the control strategy is meant to address.

3) MODE SWITCHING PERFORMANCE

To assess the performance of mode switching, the current in the transmission line is altered to define the power capability on the source side. The measured waveforms during the transition from constant-voltage to power-limited mode are presented in Figure 12.

From the waveforms captured, it is validated that the proposed feedforward strategy facilitates easy transition

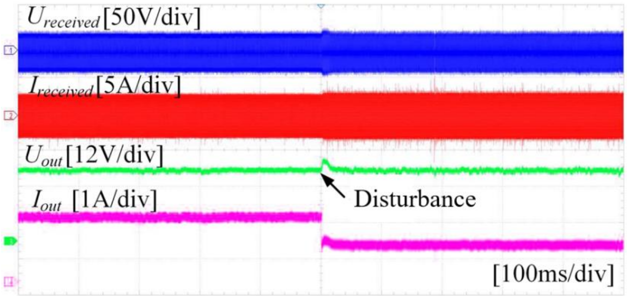

(a) Load step increase from 12 Ω to 16 Ω

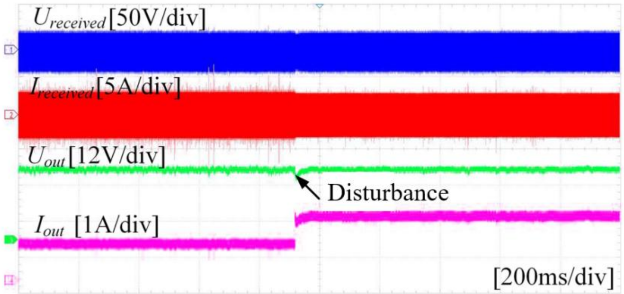

(b) Load step decrease from 16 Ω to 12 Ω

FIGURE 11. Load disturbance response under step load variation.

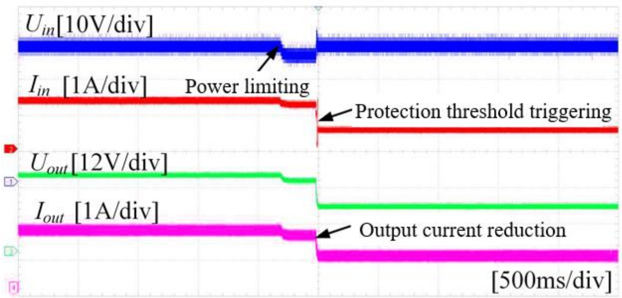

(a) Transition from constant-voltage mode to power-limited mode

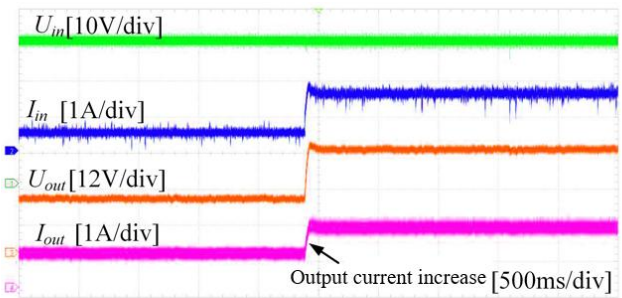

(b) Transition from power-limited mode to constant-voltage mode

FIGURE 12. Mode transition under source-side power variation.

from the constant voltage mode to power limited mode by modifying the current reference based on the source. After the power flow on the source side recovers, the system is able to transition back to constant voltage mode seamlessly.

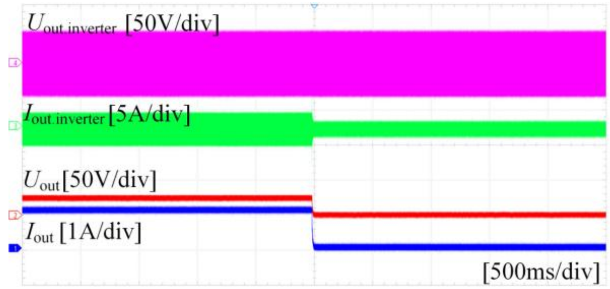

FIGURE 13. System shutdown response.

4) STEADY-STATE SHUTDOWN PERFORMANCE

To assess the performance of the steady state shutdown, a test was performed to evaluate the transient response of the system while switching it off. Measured waveforms are shown in Figure 13.

From the measured response, the output voltage and current decreased to zero seamlessly without any oscillation or random changes, which illustrates the stable performance of the control strategy during system shutdown.

V. CONCLUSION

This study analyzes the stability of a series–series compensated wireless power transfer distribution (SWPDT) system concerning source–load power fluctuation. The systematic analysis of the source-side limitation and load-side constant-voltage control interaction does an analysis of the system's source-side instabilities.

First, the author analyzes a source-side power constraint model from an energy-harvesting perspective. The author reveals the nonlinear dependence of available power on the line current and analyzes the negative impedance caused by constant-voltage control, aiding in explaining the system's intrinsic instability.

Second, through the structure of a DC bus energy balance, the author describes the dynamics of the system under a power mismatch. The author describes the positive feedback mechanism, which contributes to the collapse of the DC bus voltage, and explains its implications toward system stability.

Based on the previous analyses, the author proposes a feedforward power-constrained control strategy, which is dependent on source-side available power. Integrating control loops with source-side power capability, the author argues that system input power is constrained to be equal to the provisioned harvesting capacity. The author concludes that the proposed method diminishes demand for uncontrolled power, while improving the system's stability during source–load power fluctuations.

Finally, the author experimentally validates the SWPDT prototype regarding start-up response, load disturbance rejection, mode transition, and shutdown performance. The experimental results show improvement of DC bus voltage regulation and operational stability under changing source–load conditions.

This paper offers a theoretical approach to the instability mechanism and an accomplished control strategy for SWPDT systems, showcasing the applicability of the suggested approach for dependable energy harvesting from transmission lines.

ACKNOWLEDGEMENTS

The authors would like to acknowledge the following financial support for the research, authorship, and/or publication of this article: The authors would like to thank the Science and Technology Project of State Grid Corporation of China (J2024IC-07).

REFERENCES

[1] W. Gu, D. Qiu, X. Shu, B. Zhang, W. Xiao, and Y. Chen, “A Constant Output Capacitive Wireless Power Transfer System Based on Parity-Time Symmetric,” IEEE Transactions on Circuits and Systems II: Express Briefs, vol. 70, no. 7, pp. 2585–2589.

[2] M. Behnamfar, H. Javadi, and E. Afjei, “A dynamic CPT system LC Compensated with a six-plate capacitive coupler for wireless charging of electric vehicle in motion,” in Proc. 2020 28th Iranian Conference on Electrical Engineering (ICEE), Tabriz, Iran, pp. 1–6, 2020.

[3] Y. Guan, Y. Qiao, J. Mai, Y. Wang, and D. Xu, “Compensation Parameter Optimization of Inductive Wireless Power Transfer System for Low Stray Magnetic Field,” IEEE Transactions on Power Electronics, vol. 40, no. 5, pp. 7537–7548.

[4] F. Zhao, D. Inserra, G. Wen, J. Li, and Y. Huang, “A High-Efficiency Inverse Class-F Microwave Rectifier for Wireless Power Transmission,” IEEE Microwave and Wireless Components Letters, vol. 29, no. 11, pp. 725–728.

[5] C. Lai, C. Zhao, K. Li, D. Cai, Y. Zhang, Y. Yang, et al., “Highly efficient microwave power system of magnetrons utilizing frequency-searching injection-locking technique with no phase shifter,” IEEE Transactions on Microwave Theory and Techniques, vol. 68, no. 10, pp. 4424–4432, 2020.

[6] X. Duan, L. Zhou, Y. Zhou, Y. Tang, and X. Chen, “Short-distance wireless power transfer based on microwave radiation via an electromagnetic rectifying surface,” IEEE Antennas and Wireless Propagation Letters, vol. 19, no. 12, pp. 2344–2348, 2020.

[7] L. Liu and W. H. Abdulla, “Optimizing ultrasonic wireless power transfer systems: Theoretical and experimental analysis of piezoelectric transducer resonance,” IEEE Sensors Journal, 2025.

[8] L. Zhang, L. Tang, L. Liu, S. Zhao, M. Guo, K. Aw, and A. P. Hu, “A 2-D Equivalent Circuit Model of Ultrasonic Power Transfer Systems Considering Losses and Transducer Misalignment,” IEEE Journal of Emerging and Selected Topics in Industrial Electronics, vol. 6, no. 1, pp. 30–40, 2024.

[9] L. Liu and W. H. Abdulla, “Improving Ultrasonic Power Transfer in Air Through Hybrid S-Parameter Modeling and High-Efficiency Compensation,” Sensors, vol. 25, no. 11, Art. no. 3340, 2025.

[10] B. Peng, K. Zhang, Z. Yan, J. Wang, and Z. Mao, “An underwater anti-misalignment UPT system based on array transducers,” IEEE Journal of Emerging and Selected Topics in Power Electronics, vol. 13, no. 4, pp. 4123–4132, 2024.

[11] K. Ahmadi and W. A. Serdijn, “Advancements in laser and LED-based optical wireless power transfer for IoT applications: A comprehensive review,” IEEE Internet of Things Journal, vol. 12, no. 12, pp. 18887–18907, 2025.

[12] G. Huang, C. Liu, C. Geng, and X. Li, “Adaptive laser beam forming based on dynamic intensity transfer neural network and its application in wireless power transmission,” Optics & Laser Technology, vol. 192, Art. no. 113837, 2025.

[13] Z. Meng, Y. Xiao, L. Chen, S. Wang, Y. Fang, J. Zhou, et al., “Floating multi-focus metalens for high-efficiency airborne laser wireless charging,” Photonics, vol. 12, no. 2, Art. no. 150, Feb. 2025.

[14] K. Song, G. Yang, Y. Guo, Y. Lan, S. Dong, J. Jiang, and C. Zhu, “Design of DD coil with high misalignment tolerance and low EMF emissions for wireless electric vehicle charging systems,” IEEE Transactions on Power Electronics, vol. 35, no. 9, pp. 9034–9045, 2020.

[15] S. Wu, C. Cai, A. Wang, Z. Qin, and S. Yang, “Design and implementation of a uniform power and stable efficiency wireless charging system for autonomous underwater vehicles,” IEEE Transactions on Industrial Electronics, vol. 70, no. 6, pp. 5674–5684, 2022.

[16] C. D. Ambatali and S. Nakasuka, “Microwave wireless power transfer efficiency analysis framework for a thin film space solar power satellite,” Advances in Space Research, vol. 74, no. 1, pp. 454–470, 2024.

[17] R. Guida, E. Demirors, N. Dave, and T. Melodia, “Underwater ultrasonic wireless power transfer: A battery-less platform for the internet of underwater things,” IEEE Transactions on Mobile Computing, vol. 21, no. 5, pp. 1861–1873, 2020.

[18] D. A. Wang, S. Cui, J. Zhang, Z. Bie, K. Song, and C. Zhu, “A novel arc-shaped lightweight magnetic coupler for AUV wireless power transfer,” IEEE Transactions on Industry Applications, vol. 58, no. 1, pp. 1315–1329, 2021.

[19] A. Kurs, A. Karalis, R. Moffatt, J. D. Joannopoulos, P. Fisher, and M. Soljacic, “Wireless power transfer via strongly coupled magnetic resonances,” Science, vol. 317, no. 5834, pp. 83–86, 2007.

[20] Z. Liu, M. Su, Q. Zhu, L. Zhao, and A. P. Hu, “A dual frequency tuning method for improved coupling tolerance of wireless power transfer system,” IEEE Transactions on Power Electronics, vol. 36, no. 7, pp. 7360–7365, 2020.

[21] J. Jiang, X. Dai, and A. P. Hu, “A dynamic tuning method for ZPA frequency operation of MEU-WPT system by DC input voltages regulation,” IEEE Transactions on Power Electronics, vol. 37, no. 9, pp. 11369–11381, 2022.

[22] D. Bui, G. Wang, L. Zhao, and A. P. Hu, “A bidirectional autonomous high-frequency wireless power transfer system with constant voltage output against load and coupling variations,” IEEE Journal of Emerging and Selected Topics in Power Electronics, vol. 11, no. 6, pp. 6159–6167, 2023.

[23] M. E. Han, A. L. Li, S. A. Chowdhury, and A. P. Hu, “Mutual inductance and output voltage estimation from transmitter side of wireless power transfer by utilizing reflected third-order harmonics,” IEEE Transactions on Power Electronics, vol. 40, no. 12, pp. 18226–18236, 2025.

[24] M. E. Han, A. L. Li, S. A. Chowdhury, and A. P. Hu, “A Harmonic Suppression-Based System Identification Method for Estimating Output Voltage From the Primary-Side of Wireless Power Transfer,” IEEE Transactions on Industrial Electronics, vol. 73, no. 1, pp. 1414–1424, 2025.

[25] W. Liu, J. Lu, C. C. Mi, and K. T. Chau, “Integrated sensorless wireless charging using symmetric high-order network for multistorey car parks,” IEEE Transactions on Power Electronics, vol. 39, no. 8, pp. 10568–10581, 2024.

[26] J. Lu, G. Zhu, D. Lin, Y. Zhang, H. Wang, and C. C. Mi, “Realizing constant current and constant voltage outputs and input zero phase angle of wireless power transfer systems with minimum component counts,” IEEE Transactions on Intelligent Transportation Systems, vol. 22, no. 1, pp. 600–610, 2020.

[27] C. Cheng, T. Chen, X. Cui, Y. Liu, S. Zhang, and C. Mi, “Harmonic modeling and analysis of series-parallel compensated IPT systems with an inductive filter,” IEEE Transactions on Power Electronics, vol. 38, no. 11, pp. 13405–13414, 2023.

[28] C. Cheng, F. Lu, Z. Zhou, W. Li, C. Zhu, Z. Deng, et al., “A multiload inductive power transfer repeater system with constant load current characteristics,” IEEE Journal of Emerging and Selected Topics in Power Electronics, vol. 8, no. 4, pp. 3533–3541, 2019.

[29] T. Tan, K. Chen, Q. Lin, Y. Jiang, L. Yuan, and Z. Zhao, “Impedance shaping control strategy for wireless power transfer system based on dynamic small-signal analysis,” IEEE Transactions on Circuits and Systems I: Regular Papers, vol. 68, no. 3, pp. 1354–1365, 2020.

[30] Y. Jiang, K. Chen, Z. Zhao, L. Yuan, T. Tan, and Q. Lin, “Designing an M-shape magnetic coupler for the wireless charging system in railway applications,” IEEE Transactions on Power Electronics, vol. 37, no. 1, pp. 1059–1073, 2021.